

1
2
3
4
5
6
7
8
9
10
11
12
13
14
15
16
17
18
19
20

**Assessment of coatings for protection of cement paste against
microbial induced deterioration through image analysis**

Lijuan Kong^{a,b,c}, Jun Fang^a, Xiangming Zhou^c, Mengdi Han^a, Haoran Lu^a

^a School of Materials Science and Engineering, Shijiazhuang Tiedao University, Shijiazhuang
050043, China

^b Hebei Engineering Technology Research Center for Application of High Performance Concrete
with Ultra-low Environment Load, Shahe 054100, China

^c Department of Civil & Environmental Engineering, Brunel University London, Uxbridge,
Middlesex UB8 3PH, United Kingdom

21 **Abstract**

22 In this study, a laboratory method and equipment was developed to accelerate and study the
23 microbial induced deterioration of cementitious materials, and three types of coatings, namely,
24 cement-based capillary crystalline waterproofing coating (CCCWC), cement-based bactericidal
25 coating (CBC) and epoxy coal tar pitch coating (ECTPC) were applied onto the cement paste
26 surface, and their protecting effects were investigated. After immersion in sewage, the
27 microstructure and element distribution of cement paste were characterized by scanning electron
28 microscopy-electron dispersive spectrometry (SEM-EDS). Besides, the distribution of dead/live
29 cells within the biofilm attached to various specimens was examined by confocal scanning laser
30 microscopy (CLSM). To make a quantitative study, the image analysis was adopted. Since both
31 the images obtained belonged to RGB color system, it was found that the image processing
32 program of MATLAB is simple but very helpful for such task. The results indicate that for
33 uncoated specimen, there were the most content of S and the least contents of Ca and Si. However,
34 for coated specimens, the contents of S decreased and that of Ca and Si increased accordingly.
35 ECTPC had the best protective effect on the microbial induced deterioration of concrete, followed
36 by CBC and CCCWC. Besides the physical barrier effect, the bactericidal function of coating has
37 significant contribution for protecting concrete against sewage attack. Furthermore, the image
38 analysis was used to determine the penetration depth of element S in cement paste quantitatively,
39 and based on the change of the S concentration with penetration depth, the surface specimens can
40 be divided into three zones: interior deterioration layer, transition layer and non-corroded layer.
41 The combined use of micro-scale characterization and image analysis can provide a quick,
42 accurate and labor saving method for the deterioration study of coated concrete in sewage
43 environment.

44

45 **Keywords:** coating; cement paste; microbial induced deterioration; image analysis; MATLAB

46 1. Introduction

47 Concrete has long been used for building the municipal infrastructure due to its excellent
48 durability. However, many wastewater collection and treatment facilities face the problem of
49 concrete deterioration of its structure with time [1]. The mechanism of concrete deterioration
50 suffered from sewage attack is very complex. On top of the physical and chemical effects [2-4],
51 microbial attack is identified as a major source which induce concrete deterioration [5-8], due to
52 the harmful acids produced by the metabolic activity of many bacteria. To protect concrete
53 structures from sewage attack, surface coating is the most widely adopted measure in engineering
54 [9, 10]. Generally, the protective coatings of concrete in sewage environment can be divided into
55 two categories. One is inert coating, which isolates the concrete from aggressive acidic medium,
56 among them the acid-resistant organic resins are commonly used, such as epoxy resins, polyester
57 resins, urea formaldehyde resins, acrylic resins, polyvinyl chloride, bitumen and so on [11-14].
58 The other one is active coating, which can protect the base materials through chemical or
59 biological activities. For example, the coating prepared with inorganic or organic cementitious
60 material as the matrix and bactericide as the functional component have exhibited antibacterial or
61 bactericidal capability [15, 16].

62 Diamanti et al. [17] investigated the efficiency of two cementitious coatings modified with
63 acrylic polymers in preventing chloride-induced corrosion by testing the materials permeability to
64 water, water vapour and chlorides. Vipulanandan and Liu [18] reported the performances of two
65 commercially available polyurethane coatings under sulfuric acid environment (representing sewer
66 condition). Muynck et al. [10] and Berndt [19] adopted the accelerated microbiological tests and,
67 through measuring the macro-performance of coated concrete, found that epoxy coating has the
68 best protecting effect. Hewayde et al. [20] used the Sulfate-reducing bacteria (SRB), which were
69 isolated from an anaerobic lab-scale reactor using Desulfovibrio broth, as the medium, and found
70 that coated concrete pipes with either silver oxide or cuprous oxide effectively reduced the SRB count
71 in the nutrient solution. We can see that the effectiveness of surface coatings for protecting concrete
72 from different aggressive medium attack has been studied. However, the protecting effect of different
73 types of coatings in intensified sewage has not been systematically investigated.

74 In addition, most of the studies focused on the degradation of coatings in aggressive medium.
75 For example, Nazemi and Valix [21] investigated the diffusion and mass transfer of sulphuric acid
76 through epoxy coatings, and in order to validate the predicted result, the penetration depth of acid
77 in coating was measured by sulphur mapping of scanning electron microscopy-electron dispersive
78 spectrometry (SEM-EDS). Buenfeld and Zhang [22] observed the morphology of the polyurethane
79 coated mortar specimens after 3-year exposure to NaCl solution by SEM, and they clearly
80 observed the two-layer structure of the coating with the outer layer being much coarser than the
81 inner layer. Microbial growth inhibition and resistance to biological deterioration of concrete
82 specimens coated with silver-loaded zeolite was also studied by Haile et al. [23], the growth of *A.*
83 thiooxidans, biological sulfur oxidation, sulfate generation and biomass respiration were tested, as
84 well as the morphology and mineral compositions of concrete specimens. All of the results
85 demonstrated the resistance of silver-loaded zeolite coatings to biological sulfuric acid attack. However,
86 some properties of organic and inorganic coatings are not suitable for comparison against each
87 other. If it was possible to directly study the performance of concrete under coating, it would be
88 more accurate for assessing the protective effect of coating on concrete against sewage attack.

89 The mechanism of biodegradation and the structure of degraded cement paste specimens were
90 studied using test techniques such as, SEM, X-ray diffraction (XRD) and energy dispersive X-ray
91 analysis (EDXA) [24]. Concrete samples extracted from heavily deteriorated concrete manholes of
92 an Austrian sewer system were analyzed using microbiological, biochemical and mineralogical
93 methods [25]. The results revealed that the elemental accumulation in sample was unequivocally
94 correlated with responding pH levels, associated dissolution and precipitation of solids, as well as
95 with the spatially resolved presence of microbes. Overall, most of the current test methods to
96 assess the performance of coating and concrete are qualitative analysis based. Imaging technique
97 is a good method to characterize the degradation of both concrete and coatings intuitively. It can
98 identify the bugholes [26] and cracks [27] on concrete surface, as well as other forms of chemical
99 attack like alkali silica reaction [28] or chloride attack. Sudbrink et al. [29] and Moradillo et al. [30]
100 used micro X-ray fluorescence (μ XRF) to image the presence of silane coatings and chloride in
101 concrete samples. Jensen et al. [31] used electron probe microanalysis (EPMA) to measure
102 chloride concentration profiles in cement paste and concrete samples. In addition, SEM-EDS is

103 also frequently used in characterizing the surface chemistry of the cementitious materials [21].
104 However, to make a quantitative study, the raw data from images still need to be analyzed by
105 image processing software like toolbox of MATLAB [32, 33]. The main functions of MATLAB
106 that can be utilized include original image readin, image information collection, matrix data
107 conversion and characteristic parameters calculation, etc. In summary, the ideal method to
108 investigate the deterioration of coated concrete against sewage attack should be accurate and quick
109 with little work loading and great time saving.

110 In line with these, in this study, the artificially intensified sewage with high concentration was
111 prepared for the accelerated degradation test, and three different types of coatings were applied on
112 hardened cement paste surface. Then the change in appearance of coating and cement pastes were
113 observed in the sewage corrosion process. The techniques of SEM-EDS and confocal scanning
114 laser microscopy (CLSM) were adopted to characterize the distribution of elements and bacteria in
115 cement paste and the attached biofilm, respectively. Moreover, image analysis was used to
116 quantify the microstructure deterioration of coated and uncoated cement paste specimens. The
117 objective of the present study is to investigate and propose a reliable and labor saving method for
118 deterioration determination and mechanism analysis of coated concrete in sewage environment,
119 which helps in comparing the protective effects among different surface coatings for concrete.

120

121 2. Experimental program

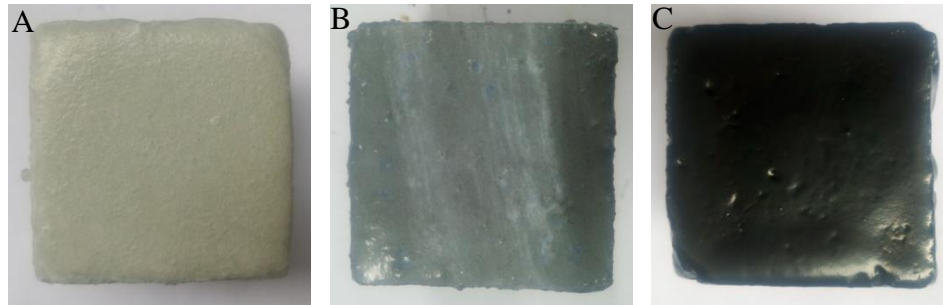
122 *2.1 Cement paste specimens*

123 Grade 42.5 Ordinary Portland Cement (Chinese standard GB175-2007) was used in the
124 production of cement paste specimens. The cement paste was prepared with a water/cement ratio
125 of 0.5 and molded in 40 mm×40 mm×40 mm cube blocks. After curing (i.e. temperature was
126 kept at 20 °C and the relative humidity was higher than 95%) for 28 days, the cement paste
127 specimens were coated with the three types of coatings, respectively.

128 *2.2 Surface coatings*

129 Three typical protective coatings for cement and concrete were investigated, including
130 cement-based capillary crystalline waterproofing coating (CCCWC), cement-based bactericidal

131 coating (CBC) and epoxy coal tar pitch coating (ECTPC), in this study as shown in Fig. 1. The
 132 specific compositions and technology of coatings investigated in this study are summarized in
 133 Table 1.



134
 135 **Fig. 1** Cement paste specimens with different coatings: A) CCCWC, B) CBC, C) ECTPC.
 136

137 **Table 1** Compositions and technology of coatings

Coatings	Mixing ratio	Coating technology	Main components	Functional component
CCCWC	Powder : water =5:2 (by mass)	2 layers of coats total 4.02 kg/m ²	Ordinary portland cement and refined quartz sand	Special active chemical substances (alkali metal salt, complex compound, etc.)
CBC	Powder : water =5:2 (by mass)	2 layers of coats total 2.78 kg/m ²	Ordinary portland cement and refined quartz sand	copper phthalocyanine : cuprous oxide : potassium nitrate =1:1:1
ECTPC	Binder : curing agent =10:1 (by mass)	4 layers of coats total 2.19 kg/m ²	epoxy resin, coal tar pitch, antirust pigment, auxiliary agent and modified amine	

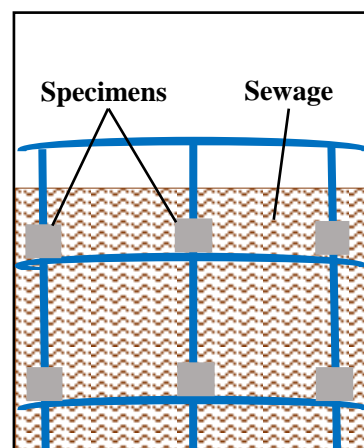
138
 139 CCCWC has obvious effect on repairing cracks through blocking pores, and can improve the
 140 impermeability and corrosion resistance of concrete. CBC has certain bactericidal capability to
 141 inhibit the production of biological acid. ECTPC can act as a barrier to isolate the concrete from
 142 aggressive acidic medium. Among them, both CCCWC and CBC are cement-based inorganic
 143 coatings. Prior to coating, they were mixed with water and stirred for 1 min with an agitator.
 144 ECTPC is a type of organic coating. According to the manufacture's guidelines, after mixing the
 145 binder with curing agent and cured for 20 minutes, the diluting agent was added, and then the
 146 coating was ready to be used after a secondary mixing. The thickness of all the three types of
 147 coating applied on cement paste specimen surface was about 4-6 mm.

148 **2.3 Sewage corrosion test**

149 In order to accelerate the test, the artificially intensified sewage with a **chemical oxygen demand**
150 **(COD)** concentration of 6000 mg/L, 20 times the concentration of ordinary sewage, was prepared
151 as follows. First, 1 kg activated sludge, which were obtained from the secondary sedimentation
152 tank in Shijiazhuang Sewage Plant, was used as the parent; then 20 kg nutrient solution, which
153 consisted of starch (200.0 g), glucose (110.0 g), peptone (28.5 g), urea (12.0 g), $(\text{NH}_4)_2\text{HPO}_4$ (6.7
154 g), MgSO_4 (3.6 g), NaCl (1.2 g), was added into the parent sewage to promote the reproduction of
155 microbes. The in-house sewage corrosion device for concrete, developed for this study, is shown
156 in Fig. 2, which was formed with a plexiglass cylindrical body (400 mm inside diameter, 8mm
157 thick). An automatic heating rod was fixed to keep the sewage at a constant temperature of 30 °C,
158 which is good for the growth and reproduction of microbes. Moreover, to prevent the
159 sedimentation of sewage and maintain a uniform and stabilized corrosive environment, a mixer
160 was fixed on the center of the device. The uncoated and all sides coated concrete specimens were
161 placed on the shelf and immersed in the sewage, thus the specimens could be corroded fully and
162 evenly as designated. The medium inside the device was replaced with the fresh nutrient solution
163 every 7 days by a pump. The total liquid removed per cycle was less than 30% of the original
164 sewage by volume. The cement paste specimens without and with different coatings were placed
165 into four separate corrosion devices.



166
167 (a) Photo of experiment device

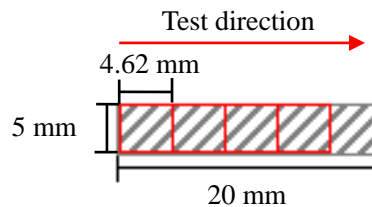


(b) Sketch of experiment device

168 **Fig. 2 Sewage corrosion device**

169 **2.4 SEM-EDS test procedure**

170 The uncoated and coated cement paste samples (with coating removed) with 10 mm thick were
171 cut from the middle of their exposed surface, and the profile had a length of approximately 20 mm
172 across the surface of each sample. Then the samples was polished by silicon carbide sandpaper of
173 180 meshes, 600 meshes and 1200 meshes, respectively, until they became as thin as about 5 mm.
174 Ethanol was then used to remove dirt and residue from the polished surface. The penetration depth
175 and relative content of sulphate in artificially intensified sewage can be determined by area
176 mapping of sulphur (S) element through the cross section of samples from outside to inside using
177 SEM-EDS. This was carried out by using Zeiss Gemini SEM 300 with a spectrometer. The
178 parameters of surface scanning were set at the acceleration voltage of 18 KV and resident time of
179 100 s. Since the maximum range that can be observed by SEM with the lowest magnification
180 factor (i.e. 25 times) is 4.62 mm, the sample was divided into the equal interval segment with a
181 conductive pen to ensure that the dividing line can be observed by SEM, as shown in Fig. 3.
182 Therefore, in this study the test range of cement paste samples were 18.48 mm. In addition, the
183 microstructures of different cement paste samples were observed at 3000 magnification, and the
184 distribution of calcium (Ca) and silicon (Si) elements were also examined.



185
186

Fig. 3 Illustration of SEM-EDS test for cement paste sample

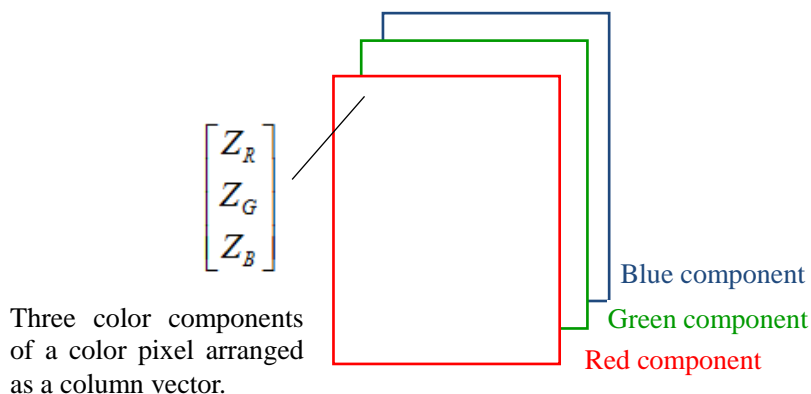
187 **2.5 CLSM test procedure**

188 The viability of bacterial cells in biofilm was determined using the live/dead cell fluorescence
189 staining kit. First, the uncoated and coated cement paste specimens were taken out from sewage,
190 and the biofilm attached to their surface was scraped down and dipped the biofilm in buffer
191 solution, which consist of NaCl (137 mmol/L), KCl (2.7 mmol/L), Na₂HPO₄ (4.3 mmol/L) and
192 KH₂PO₄ (1.4 mmol/L), to rinse off the loose cells. Then, the staining solution was prepared by
193 mixing reagent A and reagent B with the volume ratio of 1:1 and being diluted 200 times with
194 buffer solution. Finally, the microbial cells from the biofilm were stained and incubated for 5 min

195 at 37 °C , subsequently, the samples were observed under Fluoview FV-1000 CLSM. The
196 wavelengths of excitation photon and emission photon were 543 nm and 591 nm, respectively.
197 Under the blue light, the living cells exhibit green while the dead cells red.

198 **2.6 Image analysis technique**

199 The aim of image analysis is to transform a natural form of image into a digital form suitable
200 for computer processing. The pictures obtained by SEM-EDS and CLSM were all color images, so
201 they can be analyzed by the most widely used RGB color system, which is composed of three
202 monochromatic images, known as the red (R), green (G) and blue (B) component images. Each
203 component image corresponds to a two-dimensional function $f(x,y)$ [26]. Therefore, the
204 information of the image can be represented as a digital matrix in the computer, and each element
205 of the matrix has different image characteristic information [34].The schematic diagram of the
206 component pixel in RGB color image is shown in Fig. 4. MATLAB contains extensive image
207 processing tools to extract image information, which can provide simple function calls to achieve
208 that many classic image processing methods like image enhancement, image segmentation and so
209 on can achieve. In this study, the matrix representation method and the operation function of
210 image were used, which can do addition and subtraction linear operations to represent images by
211 using the form of matrix or array. To do this, first, the IMREAD function in MATLAB is used to
212 read the original image, and the information on the image is collected and the images are divided
213 into X row and Y columns according to the pixels that are read in. Then the pictures are converted
214 into matrix data based on that all the color maps are made up of the RGB matrix. Finally the
215 feature of the image is extracted and the related characteristic parameters are calculated.



216
217

Fig. 4 Schematic illustration of the image pixel in RGB color components [26]

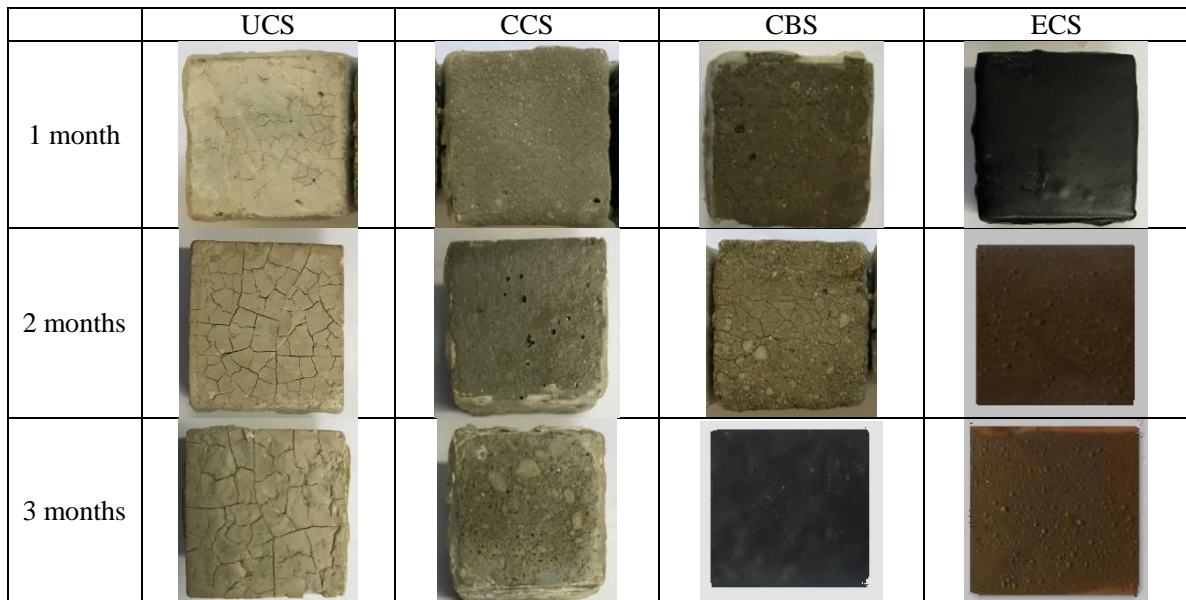
218

219 3. Results and Discussion

220 3.1 Deterioration morphology of uncoated and coated cement paste specimens

221 3.1.1 Surface morphology

222 After being immersed in sewage for 1 month, 2 months and 3 months, the surface morphology
223 of various cement paste specimens were observed, respectively, as shown in Fig. 5. The different
224 sets were designated with the following codes: uncoated cement paste specimen (UCS), cement
225 paste coated with CCCWC (CCS), cement paste coated with CBC (CBS) and cement paste coated
226 with ECTPC (ECS).



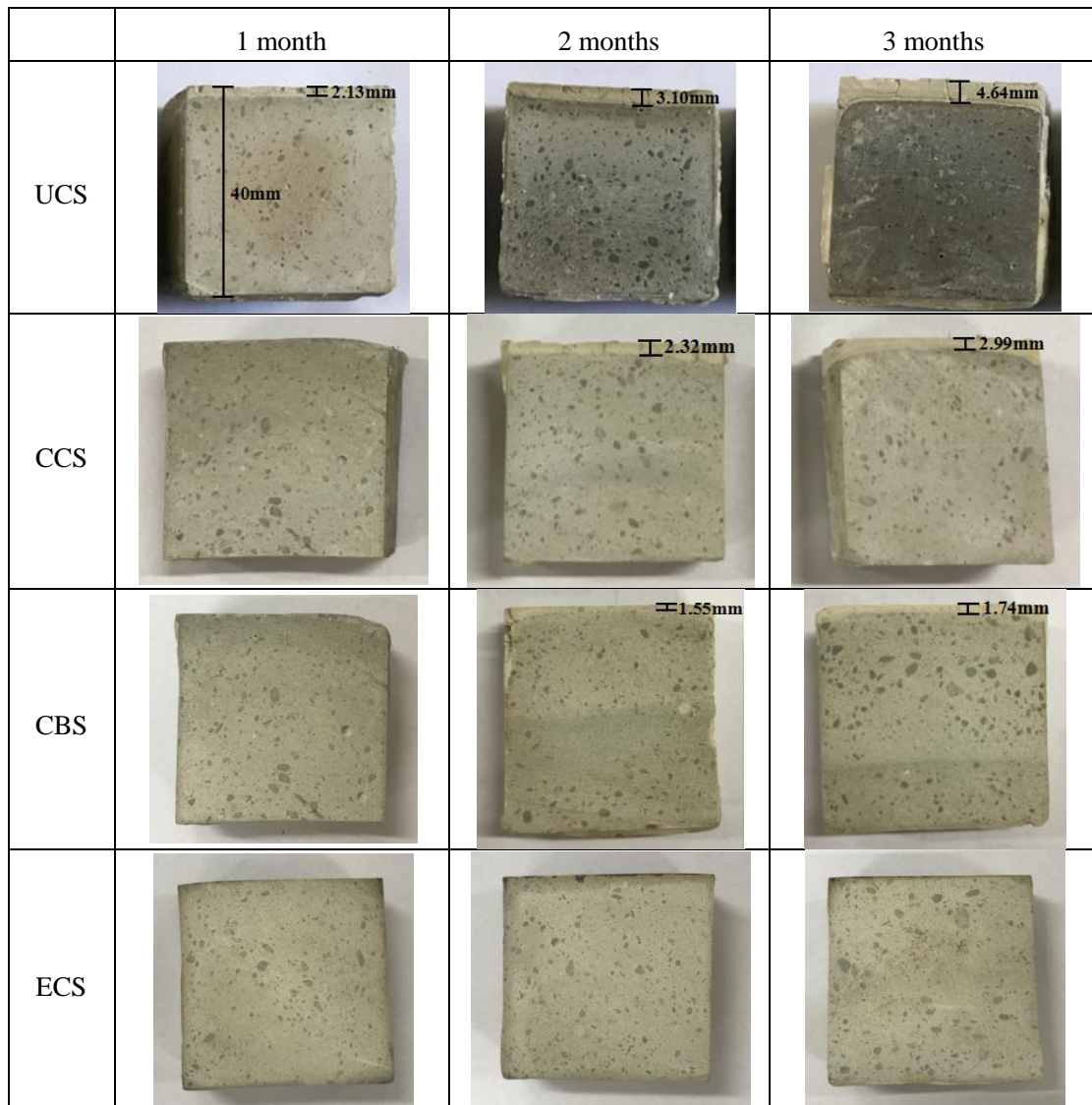
227 **Fig. 5** Surface morphology of cement paste specimens after exposure to sewage

228 It can be seen that after 1 month from the start of sewage degradation experiment, a white and
229 soft layer with many cracks was observed on the surface of UCS, whereas the appearance of other
230 three specimens had little change. With the increase of degradation time, more severe cracks
231 appeared on the surface layer of UCS, which was attributed to the formation of expansive gypsum
232 and ettringite [5, 35], and the layer was easily separated from the specimen surface. It is reported
233 that the sulfuric acid, nitric acid and organic acid produced by microbial metabolism, which can
234 react with alkali in the cement, is the main cause of concrete corrosion in sewage [36-38]. For the
235 coated specimens, the color of CCS had no significant change, whereas that of CBS and ECS had
236 changed from grey to black and from black to brown, respectively. Besides, both the inorganic

237 coatings showed signs of spalling and few cracks were observed on the surface of CBS. In
 238 comparison, the surface of CCS showed only some voids which is due to the self-healing of
 239 CCCWC. The active substance in CCCWC can enter the pores and cracks of concrete with water
 240 and react with the ions to form water-insoluble crystals [39, 40]. On the other hand, the surface of
 241 ECS showed significant amount of air bubbles with loss of gloss and swelling of the top coat.

242 *3.1.2 Section morphology*

243 In addition, the uncoated and coated cement paste specimens were cut and the coatings were
 244 stripped off using sand paper, then the cross section morphology of the samples exposed to sewage
 245 for different periods was observed, as shown in Fig. 6.



246 **Fig. 6** Section view of cement paste specimens after exposure to sewage

247 An exterior deterioration layer, which has lighter color and a sharp boundary with the cement
 248 matrix, can be seen obviously on the cross-section of all the cement paste specimens except ECS.
 249 The surface of UCS had developed a visible exterior deterioration layer after only 1 month
 250 immersion in sewage, and with the increase of time, this layer became thicker. In contrast, the
 251 exterior deterioration layers of the coated specimens of CCS and CBS were relatively thinner.
 252 However, there was no such layer observed for the coated specimen of ECS. For more accurate
 253 determination, the thickness of exterior deterioration layer of various cement paste specimens after
 254 different immersion periods were calibrated and measured by image-analysis software. The results
 255 are listed in [Table 2](#).

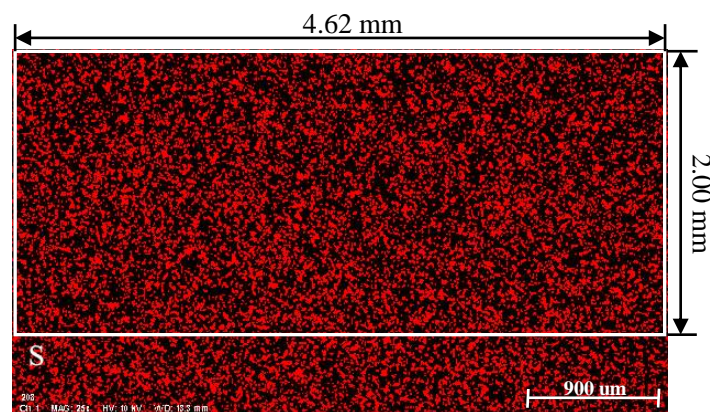
256 **Table 2** Thickness (mm) of exterior deterioration layer of different specimens

Specimens	1 month	2 months	3 months
UCS	2.13	3.10	4.64
CCS	0.00	2.32	2.99
CBS	0.00	1.55	1.74
ECS	0.00	0.00	0.00

257 **3.2 Image analysis of cement paste specimens**

258 **3.2.1 EDS images**

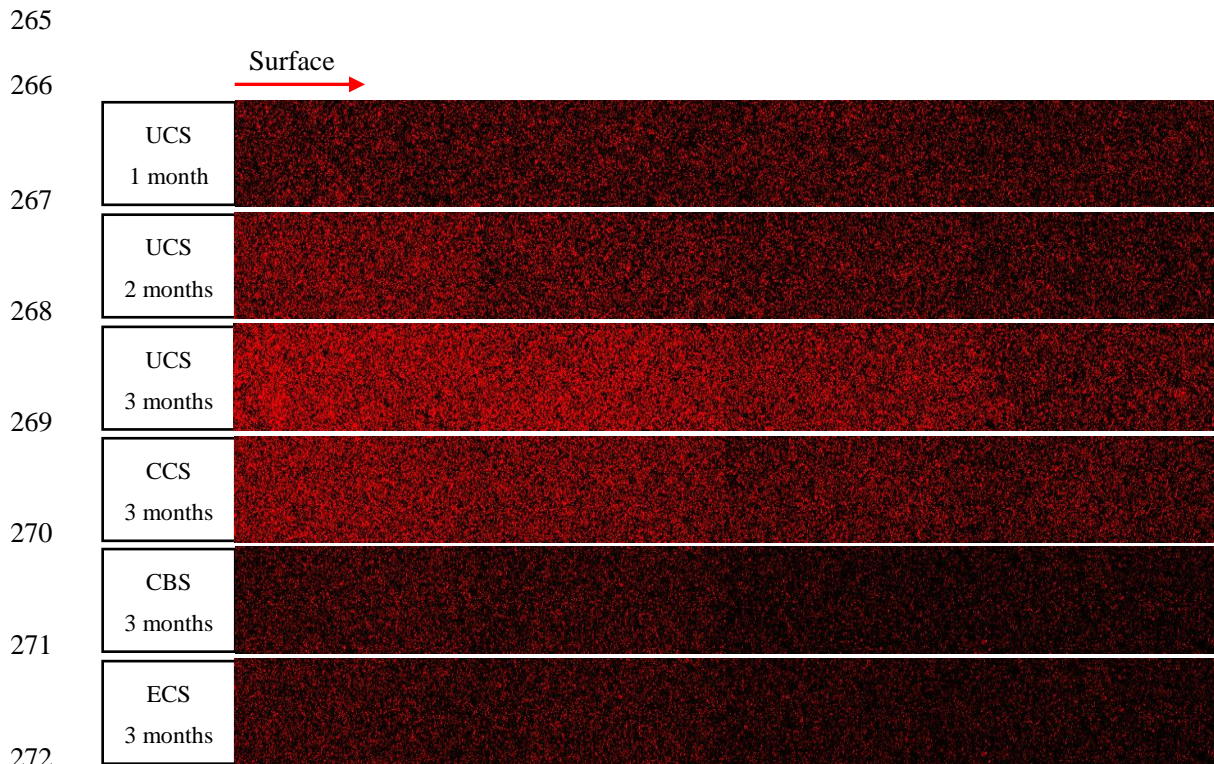
259 The area scanning image of element S in a specimen surface obtained by EDS is shown in [Fig.](#)
 260 [7](#). For each image, an area of 4.62 mm×2.00 mm was selected to eliminate the interference of
 261 other white annotations in the extraction of red pixels. Moreover, the element mappings of S
 262 throughout different cement paste specimens were stitched from 4 such images (see [Fig. 8](#)).



263

264

Fig. 7 Area scanning image of element S in cement paste by EDS



273 **Fig. 8** Sulphur profile map of cement paste specimens

274 The element distribution within the cement paste specimen was characterized by decreasing S
 275 concentration from the surface to the interior. Moreover, the S concentration within UCS increased
 276 with time, and after 3 months deterioration it became higher than that within coated specimens,
 277 especially for CBS and ECS.

278 3.2.2 MATLAB programming for image analysis

279 To make a quantitative comparison of the microstructure deterioration of coated and uncoated
 280 cement paste specimens, these EDS images were analyzed by MATLAB. Since the sulphur
 281 mapping images only contained black and red pixels, and the red pixel is $[x, 0, 0]$ and black pixel
 282 is $[0, 0, 0]$, the image analysis only involves the extraction of red pixels, which can be
 283 implemented with the MATLAB codes (see Appendix).

284 Take the specimen UCS as an example, the distribution of image pixels after one month
 285 exposure to sewage is shown in Fig. 9. It can be seen that when the pixel value was within the
 286 range of 200 to 255, and the proportion of the area of red pixels was close to 91%. For other
 287 specimens, the proportions of the area of red pixels were all above 90% within this range.
 288 Therefore, the extracted threshold pixel was set to be $[200, 255]$.

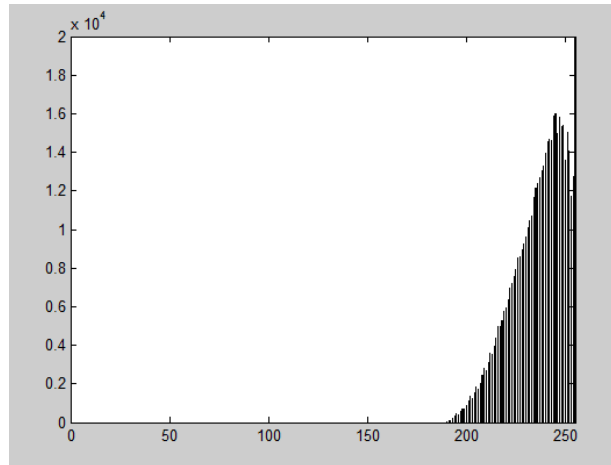


Fig. 9 Histogram of the distribution of image pixels

Besides, in order to calculate the proportion of red pixels, the image was divided into 2400 columns and 260 rows. For the sake of simplicity, set 60 columns as an interval, and the EDS image can be divided into 40 intervals, as shown in Fig. 10.

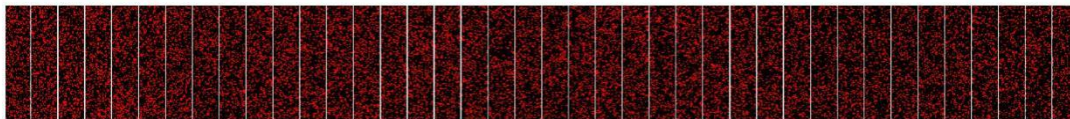


Fig. 10 Interval division of the EDS image

3.2.3 Penetration depth and content of S in specimens

According to the number of red pixels in each interval, the change of the S concentration with penetration depth in specimens can be obtained, as shown in Fig. 11. Obviously, the pixel number of S in all the specimens exhibited a fluctuating and decreasing trend. Furthermore, the test specimens were divided into three zones, which is similar to those identified by other studies [41, 42]. Zone I is described as the interior deterioration layer where significant composition and microstructure changes are expected. Zone II is described as a transition layer where moderate changes may occur. The rest of the specimen described as the non-corroded zone which is un-attacked by the sewage. In this study, only the changes in zone I and zone II were analyzed and the thicknesses of interior deterioration layer and transition layer in different specimens are listed in Table 3.

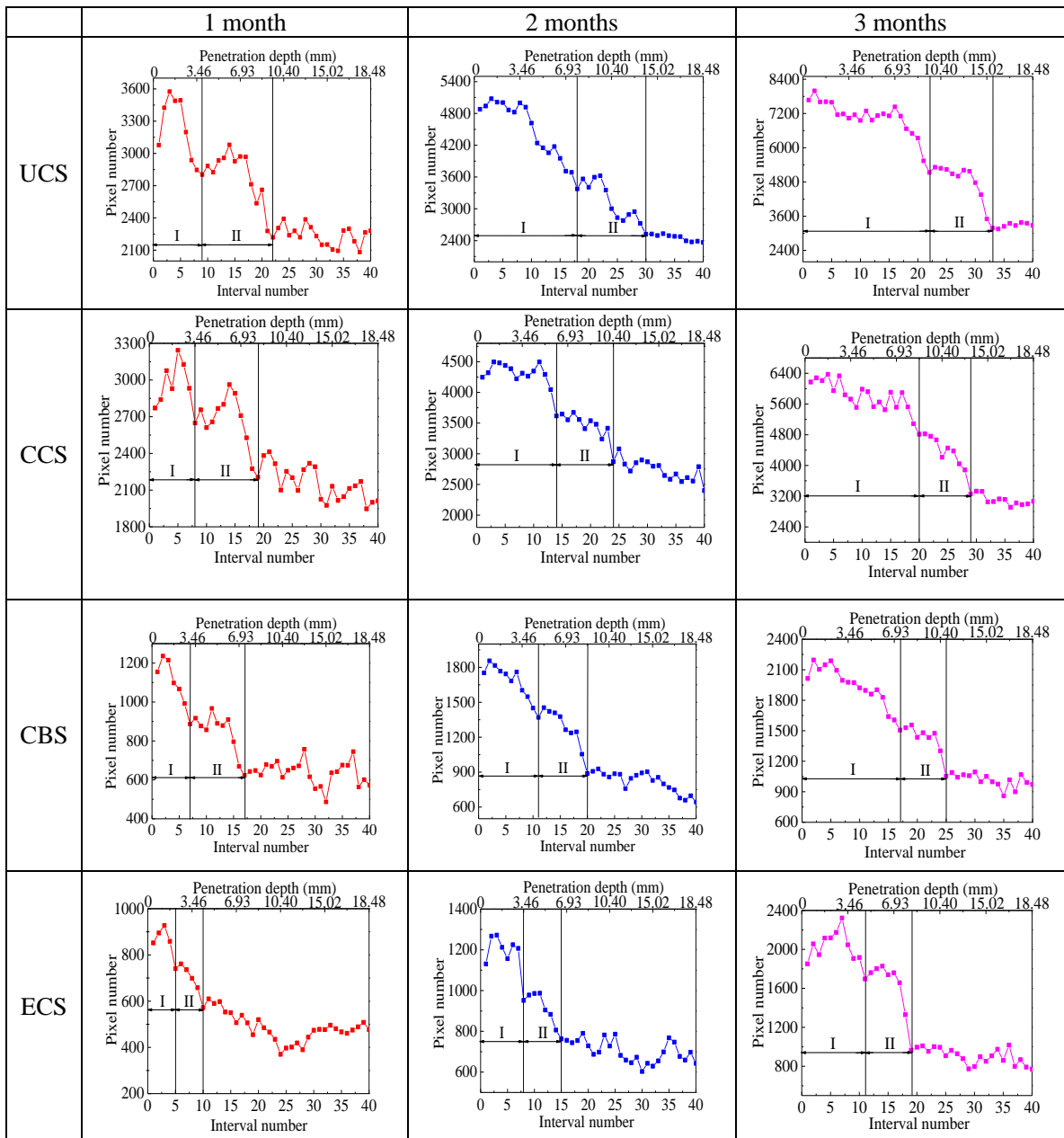


Fig. 11 Penetration depth of sulphur in cement paste specimens

308

309

It can be seen that for all the specimens, the thickness of zone I increased gradually with time,

310

whereas that of zone II decreased except ECS. This can be explained as follows. For uncoated and

311

cement based material coated specimens, the deterioration is a damage accumulation process from

312

outside to inside, and with the deterioration of structure of the surface specimens, the cracks and

313

pores formed would result in the penetration of more aggressive medium, so the deterioration rate

314

of zone I was faster than that of zone II, which led to the increase in thickness of zone I and

315

decrease in thickness of zone II with time. However, for specimen ECS, the organic coating can

316 act as a barrier to prevent sewage penetration, so it suffered the least attack by corrosive media.
 317 With the increase of immersion time, some bubbling and swelling appeared on the surface of
 318 ECTPC, which resulted in the slow penetration of sewage into a cement paste specimen, so the
 319 deterioration of specimen ECS was a gradual development process, and there was simultaneous
 320 increase in thickness of zone I and thickness of zone II with time.

321 **Table 3** Thicknesses (mm) of zone I and zone II of different specimens

Specimen	Zone I			Zone II		
	1 month	2 months	3 months	1 month	2 months	3 months
UCS	4.16	8.32	10.16	6.01	5.54	5.08
CCS	3.70	6.47	9.24	5.08	4.62	4.16
CBS	3.23	5.08	7.85	4.62	4.16	3.70
ECS	2.31	3.70	5.08	2.31	3.23	3.70

322 Based on the above study, it can be concluded that the exterior and interior deterioration layers,
 323 as well as the transition layer, all suffered sewage attack, which can be collectively referred to as
 324 the deterioration layer. So the thickness of the deterioration layer is the sum of these three items,
 325 and the results are listed in Table 4. It can be seen that the deterioration layer of uncoated
 326 specimen was significantly thicker than that of coated specimens. Moreover, these results were
 327 plotted with respect to time, as shown in Fig. 12. It can be seen that they all followed a linear
 328 relationship of Eq. (1), and the fitting parameters are listed in Table 5. The coefficients of
 329 determination (R^2) were all above 0.96, indicating that the fitting results can reflect the change of
 330 deterioration layer with time well. The slope of the fit line, which represented the relationship
 331 between deterioration layer thickness and time, can be defined as the degradation rate. Taken
 332 together, it can be seen that the UCS had both the thickest deterioration layer and the highest
 333 degradation rate. Although the deterioration layer of CCS was thinner than that of UCS, their
 334 degradation rates were similar. The deterioration layer thickness of ECS was only about one third
 335 of that of UCS, and its degradation rate was the lowest.

336
$$y = a + bx \tag{1}$$

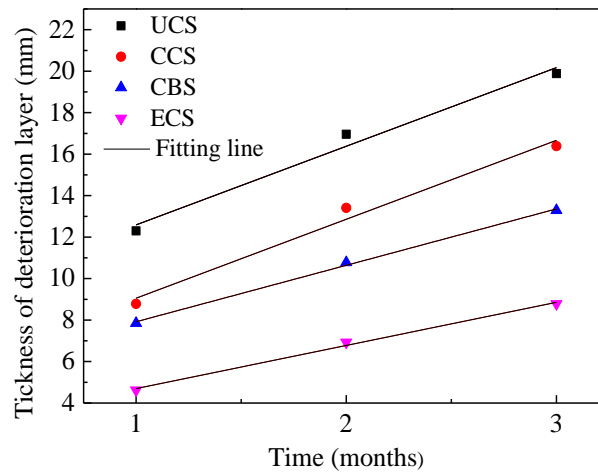
337 where x is the corrosion time in month; y is the thickness of deterioration layer in mm; and a
 338 and b are the fitting parameters.

339

Table 4 Thickness (mm) of the deterioration layer

Specimen	1 month	2 months	3 months
UCS	12.30	16.96	19.88
CCS	8.78	13.41	16.39
CBS	7.85	10.79	13.29
ECS	4.62	6.93	8.78

340



341

342

Fig. 12 Linear fitting of the change of deterioration layer thickness with time

343

Table 5 Fitting parameters of the change of deterioration layer with time

Specimen	<i>a</i>	<i>b</i>	<i>R</i> ²
UCS	8.80	3.79	0.96548
CCS	5.25	3.81	0.96914
CBS	5.20	2.72	0.99603
ECS	2.62	2.08	0.99188

344

345

In addition, the number of red pixel in the EDS image can represent the content of sulphur

346

element in cement paste specimens. From Fig. 11 it can be seen that the highest pixel number

347

appeared on the position within 3 mm of the specimen surface, and the pixel number

348

corresponding to peak of curve are listed in Table 6. The results show that the content of S element

349

in UCS was significantly higher than that in coated specimens. That is to say, the three coatings all

350

had certain effect of preventing cement paste against sewage attack, especially the organic coating,

351

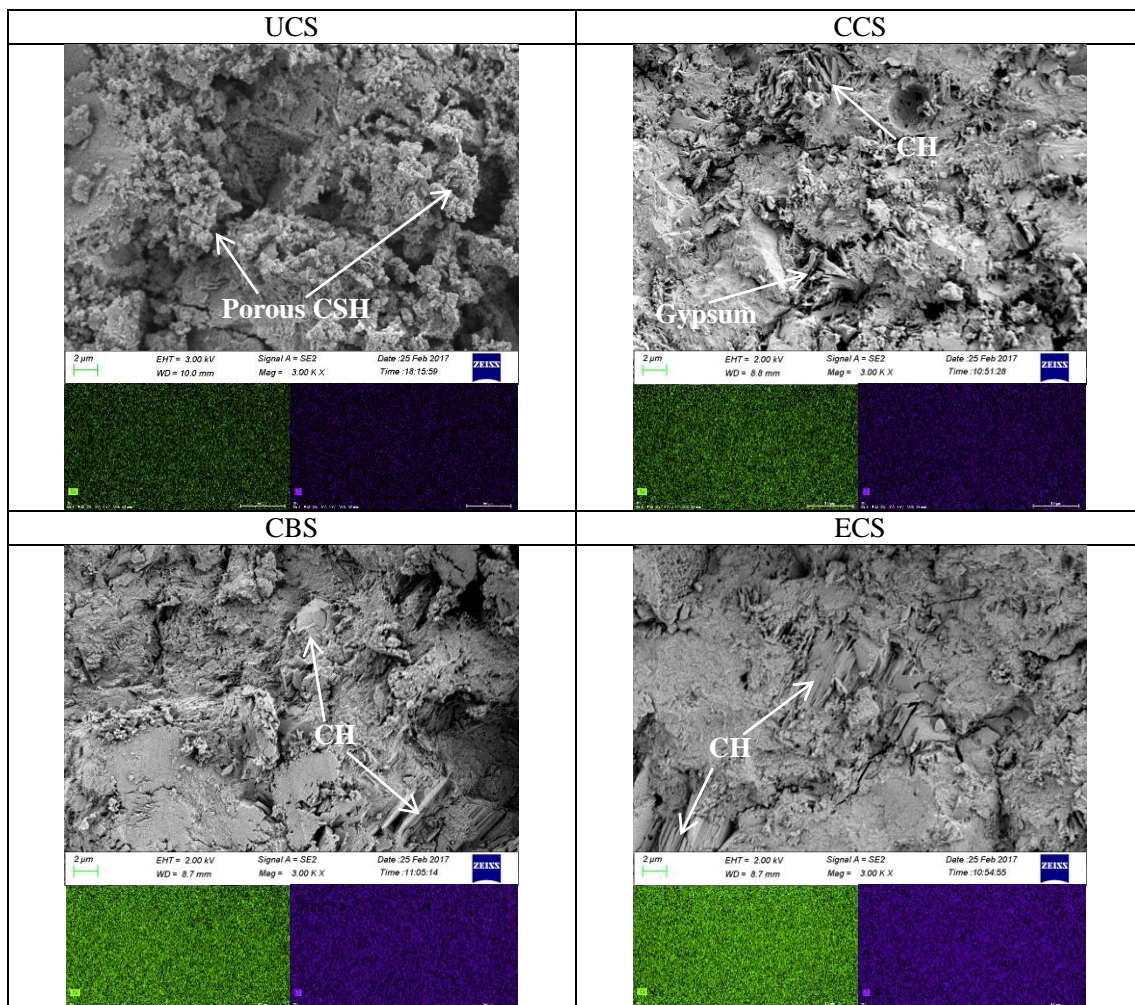
and the maximum pixel number of ECS was only about one fourth of that of UCS.

Table 6 Maximum pixel number of sulphur in cement paste specimens

Specimen	1 month	2 months	3 months
UCS	3574	5078	7992
CCS	3243	4496	6373
CBS	1236	1856	2196
ECS	927	1272	2322

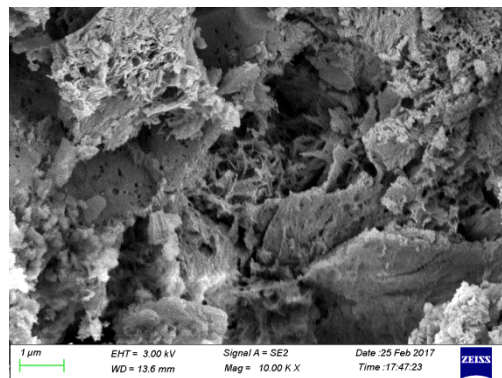
353 *3.2.4 SEM observation of specimens*

354 In order to further investigate the deterioration of cement paste specimens, the morphology and
 355 composition of uncoated and coated specimens after 2 months exposure to sewage were examined
 356 by SEM with the micrographs (taken at the depth of 5 mm from the surface of the specimens) and
 357 are shown in Fig. 13, as well the element mappings of Ca (green color) and Si (blue color).



358 **Fig. 13** SEM images and element mappings of Ca (green) and Si (blue) of specimens surface after
 359 2 months exposure to sewage

360 It can be seen that the microstructure of UCS becomes loose, and calcium hydroxide (CH)
361 crystal could barely be found. Moreover the hydrated calcium silicate (CSH) gels became very
362 porous, hence lost its binding capacity (see Fig. 14). In the micrograph of CCS, the cement paste
363 structure became denser with less CH crystal, and some short needle shaped gypsum crystals were
364 observed in the pores. In specimens CBS and ECS, some flattened CH crystals and cluster like
365 CSH gels could be observed. Such closely packed products led to the formation of a relative dense
366 structure, particularly in the case of ECS. Obviously, the deterioration of concrete microstructure
367 had been prevented by surface coatings in varying degree. From the area scanning images of
368 elements Ca and Si on each specimen surface, it can be seen that both the green and blue colors of
369 the element mappings of ECS were the brightest, followed by that of CBS, CCS and UCS,
370 indicating that the Ca and Si contents of ECS were the highest, whereas that of UCS were the
371 lowest. As it is well known, the CH and CSH are the main products of cement hydration, so the
372 decrease of the contents of Ca and Si in cement paste indicated the dissolution and consumption of
373 hydrates due to the sewage attack. This is consistent with the results obtained in S analysis.



374

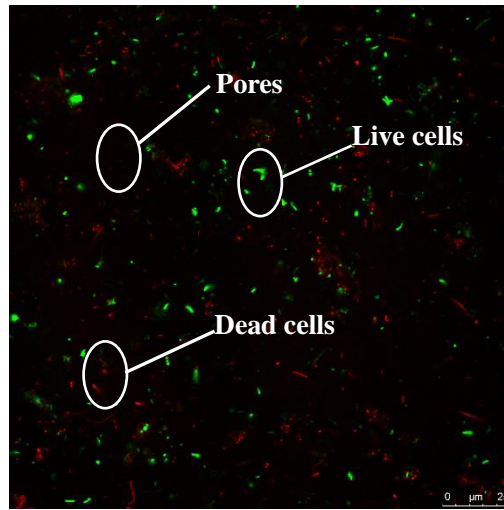
Fig. 14 SEM image of porous CSH

375

376 **3.3 Image analysis of biofilm**

377 After being immersed in sewage for one month, the bacterial colonies slowly gathered and
378 finally formed a complete and mature biofilm on the surface of uncoated and coated specimens.
379 The CLSM image is shown in Fig. 15. Under the blue light, the live cells exhibit green, the dead
380 cells exhibit red while the pores black. To further compare the distribution of dead/live cells within
381 the biofilm attached to different specimens, the images of live cells and dead cells were separated
382 (see Fig. 16) and analyzed by MATLAB, respectively. The extracted threshold pixel was set to be

383 [100, 255] by observing the histogram of the distribution of image pixels. The MATLAB code
 384 implementation process is similar to that for EDS image analysis.



385

386 **Fig. 15** CLSM image of biofilm

387

	USC	CCS	CBS	ECS
Live cells				
Dead cells				

388 **Fig. 16** Distribution of live and dead cells within the biofilm attached to different specimens

389 Based on the image analysis, the area fraction of live and dead cells within the biofilm attached
 390 to different specimens can be calculated with the results presented in [Table 7](#). By contrast, it can
 391 be found that both the numbers of live cells within the biofilms attached to UCS and CCS were
 392 higher, whereas that within the biofilms attached to CBS and ECS had a sharp decrease, especially
 393 for CBS. This is mainly due to the copper phthalocyanine and cuprous oxide that was contained in
 394 CBS, which can combine with the enzymes that required for microbes metabolism, thereby killing
 395 or inhibiting their reproduction [43]. Moreover, the coal tar pitch in ECTPC also had certain level

396 of toxicity that can destroy the microbial cell structure, and the epoxy resin can resist biological
 397 attack to a certain degree [44]. It is worth noting that although the area fraction of live cells with
 398 the biofilm attached to CBS and ECS decreased greatly, the area fraction of dead cells with them
 399 had no remarkable increase, even becoming lower than that of dead cells with the biofilm attached
 400 to UCS. This may be due to the falling-off of some dead microbes. The reduction of live cells
 401 fraction can decrease the production of extracellular polymeric substances (EPS), which is very
 402 important in promoting the microbe aggregation and structure stability.

403 **Table 7** Area fraction of live/dead cells within the biofilm attached to different specimens (%)

	UCS	CCS	CBS	ECS
Live cells	2.31	2.19	0.22	0.49
Dead cells	0.87	0.40	0.44	0.52

404 4. Conclusions

405 1. In order to propose a direct and accurate method for deterioration determination of coated
 406 concrete in sewage environment, the image analysis technique was adopted to quantitatively
 407 analyze the microbial resistance of different coatings, which is very important to the anti-sewage
 408 attack of concrete. Both the images obtained by SEM-EDS and CLSM belong to RGB color
 409 system, so the extraction of image feature was only focused on the color, and the image processing
 410 program of MATLAB can be readily used for such task.

411 2. The elemental distribution in specimens can reflect the deterioration of cement paste well.
 412 For uncoated specimen, there were higher content of S and less content of Ca and Si. However, for
 413 coated specimens, the contents of S decreased and that of Ca and Si increased accordingly. Among
 414 them, the ECTPC had the best protection effect on the microbial induced deterioration of concrete,
 415 which can be attributed to both the barrier and antibacterial effects, followed by CBC and
 416 CCCWC. This suggests that the bactericidal effect of CBC was much better than the crack
 417 self-repairing of CCCWC on protecting concrete against sewage attack.

418 3. In this study, the image analysis was used to determine the penetration depth of element S in
 419 cement paste quantitatively. Furthermore, based on the change of the S concentration with
 420 penetration depth, the surface specimens can be divided into three zones: interior deterioration

421 layer, transition layer and non-corroded layer. The combined use of micro-scale characterization
422 and image analysis can provide a quick and reliable method for the study of concrete deterioration.

423 Acknowledgements

424 This work was financially supported by the National Nature Science Foundations of China
425 (51878421), Outstanding Young People of University Science and Technology Research of Hebei
426 Province (BJ2016049) and Hebei Key Discipline Construction Project. The first author would like
427 to thank China Scholarship Council (201708130034) for sponsoring her one-year visit to Brunel
428 University London during which this paper was completed.

429

430 Appendix

431 The MATLAB script for EDS images analysis is as follows:

432 $d1 = D(:, :, 1);$ Red

433 $d2 = D(:, :, 2);$ Green

434 $d3 = D(:, :, 3);$ Blue

435 $EK = [];$

436 $EK = [];$

437 for $i = 1 : \text{length}(d1(1, :))$

438 $n=0;$

439 for $k = 1 : \text{length}(d1(:, 1))$

440 if $d1(k, i) \geq 200 \& d1(k, i) \leq 255\%$

441 $n = n+1;$

442 else

443 $n = n;$

444 end

445 end

446 $EK = [EK, n];$

447 End

448 $m = 60;$ % The interval width.

```

449     MM = [ ];
450     for j = 1 : length (EK) / m
451         s = sum (EK ((j-1) * m + 1 : (j-1) * m + m) ); % The total number of red pixels extracted
452                                                     from a single interval
453         MM = [MM, s] % The total number of red pixels in each interval
454         nn = MM / (length (d1 (:, 1) ) * m) % The proportion of red pixels in each interval
455     End
456

```

457 References

- 458 [1] M. O'Connell, C. McNally, M.G. Richardson, Biochemical attack on concrete in wastewater applications: A
459 state of the art review, *Cem. Concr. Compos.* 32 (2010) 479-485.
- 460 [2] J.Y. Han, Z.H. Gao, X.W. Zhang, Non-uniform damage of primary sedimentation pool concrete by city
461 sewage, *China J. Civil Eng.* 38 (2005) 45-49.
- 462 [3] G. Jiang, E. Wightman, The role of iron in sulfide induced corrosion of sewer concrete, *Water Res.* 49 (2014)
463 166-174.
- 464 [4] H. Yuan, P. Dangla, P. Chatellier, T. Chaussadent, Degradation modelling of concrete submitted to sulfuric
465 acid attack, *Cem. Concr. Res.* 53 (2013) 267-277.
- 466 [5] T. Mori, T. Nonaka, K. Tazaki, Interaction of nutrients, moisture and pH on microbial corrosion of concrete
467 sewer pipes, *Water Res.* 26 (1992) 29-37.
- 468 [6] E. Vinck, A. Beeldens, Chemical, microbiological, and in situ test methods for biogenic sulfuric acid
469 corrosion of concrete, *Cem. Concr. Res.* 30 (2000) 623-634.
- 470 [7] D. Nica, J.L. Davis, L. Kirby, Isolation and characterization of microorganisms involved in the
471 biodeterioration of concrete in sewers, *Int. Biodeter. Biodegr.* 46 (2000) 61-68.
- 472 [8] S. Valls, A. Yagüe, E. Vázquez, Physical and mechanical properties of concrete with added dry sludge from a
473 sewage treatment plant, *Cem. Concr. Res.* 34 (2004) 2203-2208.
- 474 [9] M. Fiertak, E. Stanaszek-Tomal, Biological corrosion of polymer-modified cement bound materials exposed
475 to activated sludge in sewage treatment plants, *Procedia Eng.* 65 (2013) 335-340.
- 476 [10] W.D. Muynck, N.D. Belle, W. Verstraete, Effectiveness of admixtures, surface treatments and antimicrobial
477 compounds against biogenic sulfuric acid corrosion of concrete, *Cem. Concr. Compos.* 31 (2009) 163-170.
- 478 [11] S.D. Jagtap, S.P. Tambe, R.N. Choudhari, B.P. Mallik, Mechanical and anticorrosive properties of non toxic
479 coal-tar epoxy alternative coating, *Prog. Org. Coat.* 77 (2014) 395-402.
- 480 [12] C. Valentini, J. Fiora, G. Ybarra, A comparison between electrochemical noise and electrochemical
481 impedance measurements performed on a coal tar epoxy coated steel in 3% NaCl, *Prog. Org. Coat.* 73 (2012)
482 173-177.
- 483 [13] M.D. Nguyen, J.W. Bang, A.S. Bin, S.R. Kim, Y. Kim, K.H. Hwang, V.H. Pham, W.T. Kwon, Novel
484 polymer-derived ceramic environmental barrier coating system for carbon steel in oxidizing environments, *J.*
485 *Eur. Ceram Soc.* 37 (2017) 2001-2010.
- 486 [14] A. Husain, O. Al-Shamah, A. Abduljaleel, Investigation of marine environmental related deterioration of
487 coal tar epoxy paint on tubular steel pilings, *Desalination.* 166 (2004) 295-304.
- 488 [15] R. Wang, K.G. Neoh, E.T. Kang, Integration of antifouling and bactericidal moieties for optimizing the

- 489 efficacy of antibacterial coatings, *J. Colloid Interf. Sci.* 438 (2015) 138-148.
- 490 [16] G. Xiao, X. Zhang, Y. Zhao, H. Su, T. Tan, The behavior of active bactericidal and antifungal coating under
491 visible light irradiation, *Appl. Surf. Sci.* 292 (2014) 756-763.
- 492 [17] M.V. Diamanti, A. Brenna, F. Bolzoni, M. Berra, T. Pastore, M. Ormellese, Effect of polymer modified
493 cementitious coatings on water and chloride permeability in concrete, *Constr. Build. Mater.* 49 (2013)
494 720-728
- 495 [18] C. Vipulanandan, J. Liu, Glass-fiber mat-reinforced epoxy coating for concrete in sulfuric acid environment,
496 *Cem. Concr. Res.* 32 (2002) 205-210
- 497 [19] M.L. Berndt, Evaluation of coatings, mortars and mix design for protection of concrete against sulphur
498 oxidising bacteria, *Constr. Build. Mater.* 25 (2011) 3893-3902
- 499 [20] E. Hewayde, G. Nakhla, E. Allouche, P. Mohan. Beneficial impact of coatings on biological generation of
500 sulfide in concrete sewer pipes, *Struct. Infrastruct. Eng.* 3 (2007) 267-277
- 501 [21] M.K. Nazemi, M. Valix, Evaluation of acid diffusion behaviour of amine-cured epoxy coatings by
502 accelerated permeation testing method and prediction of their service life, *Prog. Org. Coat.* 97 (2016)
503 307-312.
- 504 [22] N.R. Buenfeld, J.Z. Zhang. Impedance spectroscopy monitoring of a polyurethane coating on mortar exposed
505 to NaCl solution. *J. Mater. Sci.* 35 (2000) 39-44.
- 506 [23] T. Haile, G. Nakhla, E. Allouche, S. Vaidya. Evaluation of the bactericidal characteristics of nano-copper
507 oxide or functionalized zeolite coating for bio-corrosion control in concrete sewer pipes. *Corros. Sci.* 52
508 (2010) 45-53.
- 509 [24] A. Yousefi, A. Allahverdi, P. Hejazi. Accelerated biodegradation of cured cement paste by *Thiobacillus*
510 species under simulation condition. *Int. Biodeter. Biodegr.* 86 (2014) 317-326.
- 511 [25] C. Grengg, F. Mittermayr, G. Koraimann, F. Konrad, M. Szabó, A. Demenyd, M. Dietzel. The decisive role
512 of acidophilic bacteria in concrete sewer networks: A new model for fast progressing microbial concrete
513 corrosion, *Cem. Concr. Res.* 101 (2017) 93-101.
- 514 [26] B. Liu, T. Yang, Image analysis for detection of bugholes on concrete surface, *Constr. Build. Mater.* 137
515 (2017) 432-440.
- 516 [27] A. Mazzoli, S. Monosi, E.S. Plescia, Evaluation of the early-age-shrinkage of Fiber Reinforced Concrete
517 (FRC) using image analysis methods, *Constr. Build. Mater.* 101 (2015) 596-601.
- 518 [28] N. Castro, B.J. Wigum, Assessment of the potential alkali-reactivity of aggregates for concrete by image
519 analysis petrography, *Cem. Concr. Res.* 42 (2012) 1635-1644.
- 520 [29] B. Sudbrink, M.K. Moradllo, Q. Hu, M.T. Ley, J.M. Davis, N.Materer, A. Apblett, Imaging the presence of
521 silane coatings in concrete with micro X-ray fluorescence, *Cem. Concr. Res.* 92 (2017) 121-127.
- 522 [30] M.K. Moradllo, B. Sudbrink, Q. Hu, M. Aboustait, B. Tabb, M.T. Ley, J.M. Davis, Using micro X-ray

- 523 fluorescence to image chloride profiles in concrete, *Cem. Concr. Res.* 92 (2017) 128-141.
- 524 [31] O.M. Jensen, A.M. Coats, F.P. Glasser, Chloride ingress profiles measured by electron probe micro analysis,
525 *Cem. Concr. Res.* 26 (1996) 1695–1705.
- 526 [32] X. Zhu, S. Ai, D. Fang, B. Liu, X. Lu, A novel modeling approach of aluminum foam based on MATLAB
527 image processing, *Comp. Mater. Sci.* 82 (2014) 451-456.
- 528 [33] W. Deng, W. Ding, H. Zhang, Application of MATLAB in figure image processing and analysis, *J. Agr.*
529 *Mech.* 6 (2006) 194-198.
- 530 [34] B.Q. Chen, H.L. Liu, F.B. Meng, Current situation and development direction of digital image processing
531 technology, *J. Jishou Univ. Nat. Sci. Ed.* 30 (2009) 63-71.
- 532 [35] L. Kong, B. Zhang, J. Fang, Effect of bactericide on the deterioration of concrete against sewage, *J. Mater.*
533 *Civ. Eng.* 30 (2008) 1-12.
- 534 [36] A. Attal, M. Brigodiot, P. Camacho, J. Manem, Biological mechanisms of H₂S formation in sewer pipes,
535 *Water Sci. Technol.* 26 (1992) 907-914.
- 536 [37] K.S. Cho, T. Mori, A newly isolated fungus participates in the corrosion of concrete sewer pipes, *Water Sci.*
537 *Technol.* 31 (1995) 263-271.
- 538 [38] J.D. Gu, T.E. Ford, N.S. Berke, R. Mitchell, Biodeterioration of concrete by fungus *Fusarium*, *Int. Biodeter.*
539 *Biodegr.* 41 (1998) 101-109.
- 540 [39] J.Y. Yu, W.L. Li, D.X. Guo. Study on crack self-healing performance of concrete with CCCWC, *China Build.*
541 *Waterproof.* 8 (2009) 14-16.
- 542 [40] Y.C. Kuang, J.P. Ou, Experiment and Research on Permeable Crystallization Self-repairing Performance of
543 Concrete, *J. Rail. Sci. Eng.* 5 (2008) 6-10.
- 544 [41] A. Bertron, J. Duchesne, G. Escadeillas, Accelerated tests of hardened cement pastes alteration by organic
545 acids: analysis of the pH effect, *Cem. Concr. Res.* 35 (2005) 155–166.
- 546 [42] C. Grengg, F. Mittermayr, G. Koraimann, The decisive role of acidophilic bacteria in concrete sewer
547 networks: A new model for fast progressing microbial concrete corrosion, *Cem. Concr. Res.* 101 (2017)
548 93-101.
- 549 [43] H.F. Liu, L. Huang, T. Liu, H.U. Yulong, Application and progress in bactericide of sulfate reducing bacteria,
550 *J. Chin. Soc. Corros. Protect.* 29 (2009) 154-160.
- 551 [44] H.Y. Sun, Z.N. Li, S.G. Chen, Development of EA anti-microbial paint, *Mod. Paint Finish.* 4 (2002) 1-3.